PHYSICAL REVIEW D **86,** 095010 (2012)

Discovery and identification of W' and Z' in $SU(2)_1 \otimes SU(2)_2 \otimes U(1)_X$ models at the LHC

Qing-Hong Cao,[1,*] Zhao Li,[2,†] Jiang-Hao Yu,[2,‡] and C.-P. Yuan[2,3,§]

[1]*Department of Physics and State Key Laboratory of Nuclear Physics and Technology, Peking University, Beijing 100871, China*
[2]*Department of Physics and Astronomy, Michigan State University, East Lansing, Michigan 48824, USA*
[3]*Center for High Energy Physics, Peking University, Beijing 100871, China*

(Received 5 July 2012; published 8 November 2012)

We explore the discovery potential of W' and Z' boson searches for various $SU(2)_1 \otimes SU(2)_2 \otimes U(1)_X$ models at the Large Hadron Collider (LHC), after taking into account the constraints from low energy precision measurements and direct searches at both the Tevatron (1.96 TeV) and the LHC (7 TeV). In such models, the W' and Z' bosons emerge after the electroweak symmetry is spontaneously broken. Two patterns of the symmetry breaking are considered in this work: one is $SU(2)_L \otimes SU(2)_2 \otimes U(1)_X \to SU(2)_L \otimes U(1)_Y$ (breaking pattern I), another is $SU(2)_1 \otimes SU(2)_2 \otimes U(1)_Y \to SU(2)_L \otimes U(1)_Y$ (breaking pattern II). Examining the single production channel of W' and Z' with their subsequent leptonic decays, we find that the probability of detecting W' and Z' bosons in the considered models at the LHC (with 14 TeV) is highly limited by the low energy precision data constraints. We show that observing Z' alone, without seeing a W', does not rule out new physics models with non-Abelian gauge extension, such as the phobic models in breaking pattern I. Models in breaking pattern II would predict the discovery of degenerate W' and Z' bosons at the LHC.

DOI: 10.1103/PhysRevD.86.095010 PACS numbers: 12.60.Cn

I. INTRODUCTION

As remnants of electroweak symmetry breaking, extra gauge bosons exist in many new physics (NP) models, beyond the Standard Model (SM) of particle physics. According to their electromagnetic charges, extra gauge bosons are usually separated into two categories: one is named as W' (charged bosons) and another is Z' (neutral bosons). While Z' boson could originate from an additional Abelian $U(1)$ group, W' boson is often associated with an extra non-Abelian group. The minimal extension of the SM, which consists of both W' and Z' bosons, exhibits a gauge structure of $SU(2) \times SU(2) \times U(1)$ [1–13], named as $G(221)$ model [13]. Searching for those new gauge bosons [14] and determining their quantum numbers [15] would shed light on the gauge structure of NP.

At the Large Hadron Collider (LHC), it is very promising to search for those heavy Z' and W' bosons through their single production channel as an s-channel resonance with their subsequent leptonic decays [16]. It yields the simplest event topology to discover Z' and/or W' with a large production rate and clean experiment signature. These channels may be one of the most promising early discoveries at the LHC [17–20]. There have been many theoretical studies of searching for the Z' boson [21–25] and the W' boson [26–32] at the LHC. In many NP models with extended gauge groups, the W' boson emerges together with the Z' boson after symmetry breaking, and usually, the W' boson is lighter than, or as heavy as, the Z' boson. It is therefore possible to discover W' prior to Z'. More often, the masses of the W' and Z' bosons are not independent, and the same is true for their couplings to the SM fermions. Hence, the discovery potential of the W' and Z' at the LHC could be highly correlated. In this paper, we present a comprehensive study of discovery potentials of both the W' and Z' boson searches in the $G(221)$ models at the LHC.

The $G(221)$ models are the minimal extension of the SM gauge group to include both the W' and Z' bosons. The gauge structure is $SU(2) \times SU(2) \times U(1)$. The model can be viewed as the low energy effective theory of many NP models with extended gauge structure when all the heavy particles other than the W' and Z' bosons decouple. In this paper, based on a linearly realized effective theory including the $SU(2) \times SU(2) \times U(1)$ gauge group, we present the collider phenomenology related to the simplest event topology in the resonance Z' and W' processes.

In the TeV scale, different electroweak symmetry breaking patterns will induce different Z' and W' mass relations. In breaking pattern I, which has the $SU(2) \otimes U(1)$ breaking down to $U(1)_Y$, the W' mass is always smaller than the Z' mass; while in breaking pattern II, the $SU(2) \otimes SU(2)$ breaking down to $SU(2)_L$ requires the W' and Z' bosons have the same mass at tree level. This feature could assist us to distinguish these two breaking patterns after the W' and Z' bosons are discovered.

The paper is organized as follows. In Sec. II, we briefly review several typical $G(221)$ models and present the relevant couplings of W' and Z' to fermions. In Sec. III, we discuss the production cross section of the so-called sequential W' and Z' bosons in hadron collisions with the next-to-leading (NLO) QCD correction included. Based on

*qinghongcao@pku.edu.cn
†zhaoli@pa.msu.edu
‡yujiangh@msu.edu
§yuan@pa.msu.edu

the narrow width approximation, we propose a simple approach to generalize the sequential W' and Z' production cross sections to various $G(221)$ models. In Sec. IV, we present the allowed theoretical parameter space of various $G(221)$ models after incorporating indirect constraints from electroweak precision test observables (EWPTs) and direct search constraints from Tevatron and 7 TeV LHC (LHC7) data. In Sec. V, we explore the potential of the 14 TeV LHC (LHC14). Finally, we conclude in Sec. VI.

II. THE MODEL

In this section, we briefly review the $G(221)$ model and the masses and couplings of W' and Z' bosons. In particular, we consider various $G(221)$ models categorized as follows: left-right (LR) [1,2,4], leptophobic, hadrophobic, fermiophobic [5–7], ununified [8,9], and nonuniversal [10–12,33]. We also considered a widely used reference model in the experiment searches: the sequential W' model. In the LR model and sequential models, if the gauge couplings are assigned to be the same for the two $SU(2)$ gauge groups, the models are considered as the manifest left-right model (MLR), and manifest sequential model (MSQ). In the MSQ, the W' couplings to the fermion are the same as the standard model W couplings to the fermion, which served as the reference model in the experiment searches. We focus our attention on the couplings of the extra gauge boson to SM fermions which are involved in extra gauge boson production via the s-channel process. More details of the $G(221)$ model can be found in our previous paper [13].

The classification of $G(221)$ models is based on the pattern of symmetry breaking and quantum number assignment of the SM fermions. The NP models mentioned above can be categorized into two symmetry breaking patterns:

(a) breaking pattern I (BP-I):
$SU(2)_1$ is identified as the $SU(2)_L$ of the SM. The first stage of symmetry breaking $SU(2)_2 \times U(1)_X \to U(1)_Y$ occurs at the TeV scale, while the second stage of symmetry breaking $SU(2)_L \times U(1)_Y \to U(1)_{\rm em}$ takes place at the electroweak scale;

(b) breaking pattern II (BP-II):
$U(1)_X$ is identified as the $U(1)_Y$ of the SM. The first stage of symmetry breaking $SU(2)_1 \times SU(2)_2 \to SU(2)_L$ occurs at the TeV scale, while the second stage of symmetry breaking $SU(2)_L \times U(1)_Y \to U(1)_{\rm em}$ happens at the electroweak scale.

The symmetry breaking is assumed to be induced by fundamental scalar fields throughout this paper. The quantum number of the scalar fields under the $G(221)$ gauge group depends on the breaking pattern. In BP-I, the symmetry breaking of $SU(2)_2 \otimes U(1)_X \to U(1)_Y$ at the TeV scale could be induced by a scalar doublet field $\Phi \sim (1,2)_{1/2}$, or a triplet scalar field $(1,3)_1$ with a vacuum expectation value (VEV) u, and the subsequent symmetry breaking of $SU(2)_1 \otimes U(1)_Y \to U(1)_Q$ at the electroweak scale is via another scalar field $H \sim (2,\bar{2})_0$ with two VEVs v_1 and v_2, which can be redefined as a VEV $v = \sqrt{v_1^2 + v_2^2}$ and a mixing angle $\beta = \arctan(v_1/v_2)$. In BP-II, the symmetry breaking of $SU(2)_1 \otimes SU(2)_2 \to SU(2)_L$ at the TeV scale is owing to a Higgs bidoublet $\Phi \sim (2,\bar{2})_0$ with only one VEV u, and the subsequent breaking of $SU(2)_L \otimes U(1)_Y \to U(1)_Q$ at the electroweak scale is generated by a Higgs doublet $H \sim (2,1)_{1/2}$ with the VEV v. Since the precision data constraints (including those from CERN LEP and SLAC SLC experiment data) pushed the TeV symmetry breaking higher than 1 TeV, we shall approximate the predictions of physical observables by taking Taylor expansion in $1/x$ with $x = u^2/v^2$, which is assumed to be much larger than 1.

Denote g_1, g_2, and g_X as the coupling of $SU(2)_1$, $SU(2)_2$, and $U(1)_X$, respectively. Depending on the symmetry breaking pattern, the three couplings are

$$g_1 = \frac{e}{s_W}, \qquad g_2 = \frac{e}{c_W s_\phi}, \qquad g_X = \frac{e}{c_W c_\phi}, \qquad \textbf{(BP-I)}, \tag{1}$$

$$g_1 = \frac{e}{s_W c_\phi}, \qquad g_2 = \frac{e}{s_W s_\phi}, \qquad g_X = \frac{e}{c_W}, \qquad \textbf{(BP-II)}, \tag{2}$$

where s_W and c_W are sine and cosine of the SM weak mixing angle, while s_ϕ and c_ϕ are sine and cosine of the new mixing angle ϕ appearing after the TeV symmetry breaking.

After symmetry breaking, both W' and Z' bosons obtain masses and mix with the SM gauge bosons. The masses of the W' and Z' are given as follows:

(i) In BP-I, we find

$$M^2_{W'^\pm} = \frac{e^2 v^2}{4 c_W^2 s_\phi^2}(x+1), \tag{3}$$

$$M^2_{Z'} = \frac{e^2 v^2}{4 c_W^2 s_\phi^2}(x + c_\phi^4). \tag{4}$$

(ii) In BP-II, we notice that the masses of the W' and Z' bosons are degenerated at the tree level, and

$$M^2_{W'^\pm} = M^2_{Z'} = \frac{e^2 v^2}{4 s_W^2 s_\phi^2 c_\phi^2}(x + s_\phi^4). \tag{5}$$

Now, consider the gauge interaction of W' and Z' to the SM fermions. Note that throughout this work, only SM fermions are considered, despite that in certain models new heavy fermions are necessary to cancel gauge anomalies. Study of W' and Z' bosons in a UV completion theory is

certainly interesting but beyond the scope of this paper. Charge assignments of SM fermions in those models of our interest are listed in Table I.

The most general interaction of the Z' and W' to SM fermions is

$$\mathcal{L}_f = g_2 Z'_\mu \bar{f}\gamma^\mu(g_L P_L + g_R P_R)f + g_2 W'_\mu \bar{f}\gamma^\mu(g'_L P_L + g'_R P_R)f' + \text{H.c.}, \quad (6)$$

where $g_2 = e/\sin\theta$ is the weak coupling strength and $P_{L,R} = (1 \mp \gamma_5)/2$ are the usual chirality projectors. For simplicity, we use g_L and g_R for both Z' and W' bosons from now on. Detailed expressions of g_L and g_R for each individual NP model are listed in Table II. According to Tables I and II, the couplings of W' to fermions (either leptons or quarks) are suppressed in the fermiophobic (either leptophobic or hadrophobic) model, while the couplings of Z' to fermions (either leptons or quarks) are not.

Triple gauge boson couplings as well as the scalar-vector-vector couplings are also listed as they arise from the symmetry breaking and may contribute to the W' and Z' decay.

III. W' AND Z' PRODUCTION AND DECAY

A. V' production at the LHC

At the LHC, the cross section of $pp \to V' \to \bar{f}f'$ ($V' = W'/Z'$) is

$$\sigma_{pp\to V'\to\bar{f}f'} = \sum_{\{ij\}} \int_{\tau_0}^1 \frac{d\tau}{\tau}\cdot\frac{1}{s}\frac{d\mathcal{L}_{ij}}{d\tau}\cdot[\hat{s}\hat{\sigma}_{ij\to V'\to\bar{f}f'}(\hat{s})], \quad (7)$$

where $\sqrt{s}$ is the total energy of the incoming proton-proton beam, $\sqrt{\hat{s}}$ is the partonic center-of-mass energy, and $\tau \equiv \hat{s}/s$. The lower limit of the τ variable is determined by the kinematics threshold of the V' production, i.e., $\tau_0 = M^2_{V'}/s$. The parton luminosity $\frac{1}{s}\frac{d\mathcal{L}_{ij}}{d\tau}$ is defined as

$$\frac{1}{s}\frac{d\mathcal{L}_{ij}}{d\tau} = \frac{1}{1+\delta_{ij}}\frac{1}{s}\int_\tau^1 \frac{dx}{x}[f_i^{(a)}(x)f_j^{(b)}(\tau/x) + f_j^{(a)}(x)f_i^{(b)}(\tau/x)], \quad (8)$$

where i and j denote the initial state partons and $f_i^{(a)}(x)$ is the parton distribution of the parton i inside the hadron a with a momentum fraction of $x = p_i/p_a$. Using the narrow width approximation, one can factorize the $pp \to V' \to \bar{f}f'$ process into the V' production and the V' decay,

$$\sigma_{pp\to V'\to\bar{f}f'} = \left(\sum_{\{ij\}}\int_{\tau_0}^1 \frac{d\tau}{\tau}\cdot\frac{1}{s}\frac{d\mathcal{L}_{ij}}{d\tau}\cdot[\hat{s}\hat{\sigma}_{ij\to V'}(\hat{s})]\right) \times \text{Br}(V' \to \bar{f}f'), \quad (9)$$

where the branching ratio (Br) is defined as $\text{Br}(V' \to \bar{f}f') = \Gamma(V' \to \bar{f}f')/\Gamma_{\text{tot}}$. As to be shown later, the decay widths of Z' and W' bosons in most of the allowed parameter space are much smaller than their masses, which validates the narrow width approximation adapted in this work.

TABLE I. Assignment of SM fermions under the $G(221)$ symmetry: $(T_L, T_R)_X$ in breaking pattern I while $(T_l, T_h)_Y$ in breaking pattern II. Unless otherwise specified, the fermion doublet represents three generations of SM fermions. LRD (LRT) denotes the left-right doublet (triplet) model, where the $G(221)$ model is broken by a scalar doublet (triplet). Similarly, LPD (LPT) denotes the leptophobic doublet (triplet) model, HPD (HPT) the hadrophobic doublet (triplet) model, FPD (FPT) the fermiophobic doublet (triplet) model, SQD the sequential W' model with doublet Higgs, TFD the nonuniversal doublet model, while UUD is the ununified doublet model.

Models	$SU(2)_1$ (T_L, T_l)	$SU(2)_2$ (T_R, T_h)	$U(1)_X$ (X, Y)
LRD/LRT	$\begin{pmatrix}u_L\\d_L\end{pmatrix}, \begin{pmatrix}\nu_L\\e_L\end{pmatrix}$	$\begin{pmatrix}u_R\\d_R\end{pmatrix}, \begin{pmatrix}\nu_R\\e_R\end{pmatrix}$	$X_q = 1/6\ X_l = -1/2$
LPD/LPT	$\begin{pmatrix}u_L\\d_L\end{pmatrix}, \begin{pmatrix}\nu_L\\e_L\end{pmatrix}$	$\begin{pmatrix}u_R\\d_R\end{pmatrix}$	$X_q = 1/6\ X_l = Y_{\text{SM}}$
HPD/HPT	$\begin{pmatrix}u_L\\d_L\end{pmatrix}, \begin{pmatrix}\nu_L\\e_L\end{pmatrix}$	$\begin{pmatrix}\nu_R\\e_R\end{pmatrix}$	$X_q = Y_{\text{SM}}\ X_l = -1/2$
FPD/FPT	$\begin{pmatrix}u_L\\d_L\end{pmatrix}, \begin{pmatrix}\nu_L\\e_L\end{pmatrix}$		$X_f = Y_{\text{SM}}$
SQD	$\begin{pmatrix}u_L\\d_L\end{pmatrix}, \begin{pmatrix}\nu_L\\e_L\end{pmatrix}$		$X_f = Y_{\text{SM}}$
TFD	$\begin{pmatrix}u_L\\d_L\end{pmatrix}_{1st,2nd}, \begin{pmatrix}\nu_L\\e_L\end{pmatrix}_{1st,2nd}$	$\begin{pmatrix}u_L\\d_L\end{pmatrix}_{3rd}, \begin{pmatrix}\nu_L\\e_L\end{pmatrix}_{3rd}$	$X_f = Y_{\text{SM}}$
UUD	$\begin{pmatrix}u_L\\d_L\end{pmatrix}$	$\begin{pmatrix}\nu_L\\e_L\end{pmatrix}$	$X_f = Y_{\text{SM}}$

TABLE II. The fermion couplings and triple boson couplings of the heavy gauge boson in Breaking Pattern I and II. For the fermion couplings, the quantum numbers (T_L, T_R) in BP-I and (T_l, T_h) in BP-II are implied in Table I, and is given in our previous paper [13]. In BP-II, the fermion notation f means the fermions listed in the column $SU(2)_1$, while F means the fermions listed in the column $SU(2)_2$ in Table I. For the triple gauge boson couplings, the Lorentz index $[g^{\mu\nu}(k_1-k_2)^\rho + g^{\nu\rho}(k_2-k_3)^\mu + g^{\rho\mu}(k_3-k_1)^\nu]$ is implied.

Couplings	g_L	g_R
$W'^{+\mu}\bar{f}f'$ (BP-I)	$-\frac{e_m}{\sqrt{2}s_W^2}\gamma_\rho T_L^+ \frac{c_W s_{2\beta} s_\phi}{x}$	$\frac{e_m}{\sqrt{2}c_W s_\phi}\gamma_\rho T_R^+$
$Z'\bar{f}f$ (BP-I)	$\frac{e_m}{c_W c_\phi s_\phi}\gamma_\rho\left[(T_{3L}-Q)s_\phi^2 - \frac{c_\phi^4 s_\phi^2 (T_{3L}-Qs_W^2)}{x s_W^2}\right]$	$\frac{e_m}{c_W c_\phi s_\phi}\gamma_\rho\left[(T_{3R}-Qs_\phi^2) + Q\frac{c_\phi^4 s_\phi^2}{x}\right]$
$W'^{\pm\mu}\bar{f}f'$ (BP-II)	$-\frac{e_m s_\phi}{\sqrt{2}s_W c_\phi}\gamma^\mu T_l^\pm\left(1+\frac{s_\phi^2 c_\phi^2}{x}\right)$	0
$W'^{\pm\mu}\bar{F}F'$ (BP-II)	$\frac{e_m c_\phi}{\sqrt{2}s_W s_\phi}\gamma^\mu T_h^\pm\left(1-\frac{s_\phi^4}{x}\right)$	0
$Z'\bar{f}f$ (BP-II)	$-\frac{e_m}{s_W}\gamma^\mu\left[\frac{s_\phi}{c_\phi}T_{3l}(1+\frac{s_\phi^2 c_\phi^2}{x c_W^2}) - \frac{s_\phi}{c_\phi}\frac{s_\phi^2 c_\phi^2}{x c_W^2}s_W^2 Q\right]$	$\frac{e_m}{s_W}\gamma^\mu\left(\frac{s_\phi}{c_\phi}\frac{s_\phi^2 c_\phi^2}{x c_W^2}s_W^2 Q\right)$
$Z'\bar{F}F$ (BP-II)	$\frac{e_m}{s_W}\gamma^\mu\left[\frac{c_\phi}{s_\phi}T_{3h}(1-\frac{s_\phi^4}{x c_W^2}) + \frac{c_\phi}{s_\phi}\frac{s_\phi^4}{x c_W^2}s_W^2 Q\right]$	$\frac{e_m}{s_W}\gamma^\mu\left(\frac{c_\phi}{s_\phi}\frac{s_\phi^4}{x c_W^2}s_W^2 Q\right)$
Couplings	BP-I	BP-II
$HW_\nu W'_\rho$	$-\frac{i}{2}\frac{e_m^2 s_{2\beta}}{c_W s_W s_\phi}\upsilon g_{\nu\rho}\left[1+\frac{(c_W^2 s_\phi^2 - s_W^2)}{x s_W^2}\right]$	$-\frac{i}{2}\frac{e_m^2 s_\phi}{s_W^2 c_\phi}\upsilon g_{\nu\rho}\left[1+\frac{s_\phi^2(c_\phi^2-s_\phi^2)}{x}\right]$
$HZ_\nu Z'_\rho$	$-\frac{i}{2}\frac{e_m^2 c_\phi}{c_W^2 s_W s_\phi}\upsilon g_{\nu\rho}\left[1-\frac{c_\phi^2(c_\phi^2 s_W^2 - s_\phi^2)}{x s_W^2}\right]$	$-\frac{i}{2}\frac{e_m^2 s_\phi}{c_W s_W^2 c_\phi}\upsilon g_{\nu\rho}\left[1-\frac{s_\phi^2(s_\phi^2 c_W^2 - c_\phi^2)}{x c_W^2}\right]$
$W_\mu^+ W_\nu^{\prime -} Z_\rho$	$i\frac{e_m s_{2\beta} s_\phi}{x s_W^2}$	$i\frac{e_m c_\phi s_\phi^3}{x s_W c_W}$
$W_\mu^+ W_\nu^- Z'_\rho$	$i\frac{e_m s_\phi c_W c_\phi^3}{x s_W^2}$	$i\frac{e_m c_\phi s_\phi^3}{x s_W}$

At NLO, the partonic cross section of the V' production is

$$\hat{\sigma}_{ij\to V'}(\hat{s}) = \frac{\pi}{6\hat{s}} g_2^2 (g_L^2 + g_R^2) H_{ij}\left(\frac{M_{V'}^2}{\hat{s}}\right), \tag{10}$$

where the functions $H_{ij}(z)$ for different parton flavors $ij = (\bar{q}q', qg, \bar{q}g)$ are

$$H_{\bar{q}q'}(z) = \delta(1-z) + \frac{\alpha_s}{2\pi}C_F\left[\left(\frac{2\pi^2}{3}-8\right)\delta(1-z) - \frac{2(1+z^2)}{1-z}\log(z) + 4(1+z^2)\left(\frac{\log(1-z)}{1-z}\right)_+\right], \tag{11}$$

and

$$H_{qg}(z) = H_{\bar{q}g}(z) = \frac{\alpha_s}{2\pi}T_F\left[(z^2+(1-z)^2)\log\frac{(1+z)^2}{z} + \frac{1}{2} + 3z - \frac{7}{2}z^2\right]. \tag{12}$$

Here, C_F and T_F are the color factor defined as $C_F = 4/3$ and $T_F = 1/2$.

It is convenient to parametrize the V' production cross section into one model-dependent piece $C_q^{V'}$ and another model-independent piece $F_q^{V'}(M_{V'}, \sqrt{s})$. The first piece consists of model couplings, while the second piece, which includes all the hadronic contributions [22], depends only on $m_{V'}$ and $\sqrt{s}$. We separate the up-quark and down-quark contributions in the Z' production because Z' couples differently to up and down quarks in most NP models. The NLO cross sections of Z' and W' production can then be expressed as

$$\sigma_{pp\to Z'\to ff} = \frac{\pi}{18s}[C_u^{Z'}F_u^{Z'}(M_{V'},\sqrt{s}) + C_d^{Z'}F_d^{Z'}(M_{V'},\sqrt{s})],$$
$$\sigma_{pp\to W'\to ff'} = \frac{\pi}{18s}[C_q^{W'}F_q^{W'}(M_{V'},\sqrt{s})], \tag{13}$$

where

$$C_q^{V'} = g_2^2(g_L^2+g_R^2)\times \mathrm{Br}(V'\to ff'), \tag{14}$$

$$F_q^{V'}(M_{V'},\sqrt{s}) = \int_{\tau_0}^1 \frac{d\tau}{\tau}\cdot\left[\frac{d\mathcal{L}_{\bar{q}q'}}{d\tau}\cdot H_{\bar{q}q'}(z) + \frac{d\mathcal{L}_{\bar{q}g}}{d\tau}\cdot H_{\bar{q}g}(z) + (\bar{q}\to q)\right]. \tag{15}$$

Note that the decay branching ratio is allocated to the model-dependent piece $C_q^{V'}$. After convoluting with parton distribution functions, the model-independent piece $F_q^{V'}$ is merely a function of $m_{V'}$ and the collider energy $\sqrt{s}$.

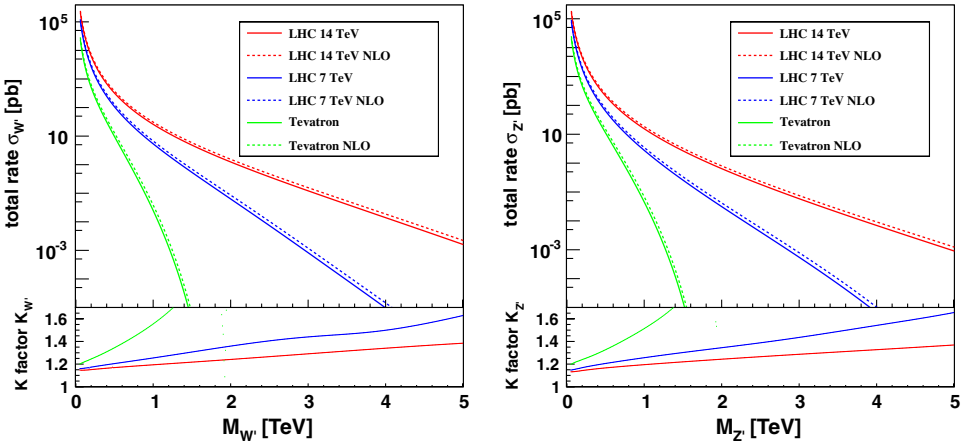

FIG. 1 (color online). Upper panel: the LO and NLO cross sections of $pp \to W'$ (left) and $pp \to Z'$ (right) process with a SM-like coupling as a function of new heavy gauge boson mass ($m_{V'}$, $V = W, Z$) in hadron collisions. Lower panel: the K factor as a function of $m_{V'}$.

Because the model-dependent couplings can be factorized out, the total cross section in the sequential W' and Z' models can be used as the reference cross section. The upper panels of Fig. 1 show the leading order (LO) and NLO production cross sections of the sequential W' (left) and Z' boson (right) as a function of the extra gauge boson mass at the Tevatron, the 7 TeV and 14 TeV LHC. The lower panels display the K factor, defined as the ratio of the NLO to LO cross sections. In the upper panels of Fig. 2, we plot the cross section of Z' production induced by the $u\bar{u}$ (left) and $d\bar{d}$ (right) initial state, respectively. Again, the lower panels show the corresponding K factors. Note that the K factors are model-independent once one separates the up-quark and down-quark contributions in the Z' production. The K factor is defined as

$$K_q = \frac{\sigma_{\rm NLO}}{\sigma_{\rm LO}} = \frac{F_q^{V'}(M_{V'}, \sqrt{s})_{\rm NLO}}{F_q^{V'_{\rm seq}}(M_{V'}, \sqrt{s})_{\rm LO}}. \tag{16}$$

Here, we adopt the CTEQ6.6M parton distribution package [34] for both the LO and NLO calculations. Both the factorization and renormalization scales are set to be $M_{V'}$.

The NLO cross section of other NP models can be obtained easily from the sequential W' and Z' cross sections plotted in Figs. 1 and 2 by

(i) scaling the model-dependent $C^{V'}$-coefficients $(C_u^{Z'}/C_u^{Z'_{\rm seq}}, C_d^{Z'}/C_d^{Z'_{\rm seq}}, C_q^{W'}/C_q^{W'_{\rm seq}})$,

(ii) including the NLO QCD correction with the inclusive K factors (K_u, K_d and K_q).

To be more specific, the NLO cross sections of new gauge boson productions in the $G(221)$ model are

$$\sigma_{W'} = \frac{C_q^{W'}}{C_q^{W'_{\rm seq}}}(F_q^{W'})_{\rm LO} \times K_q,$$
$$\sigma_{Z'} = \frac{C_u^{Z'}}{C_u^{Z'_{\rm seq}}}(F_u^{Z'})_{\rm LO} \times K_u + \frac{C_d^{Z'}}{C_d^{Z'_{\rm seq}}}(F_d^{Z'})_{\rm LO} \times K_d. \tag{17}$$

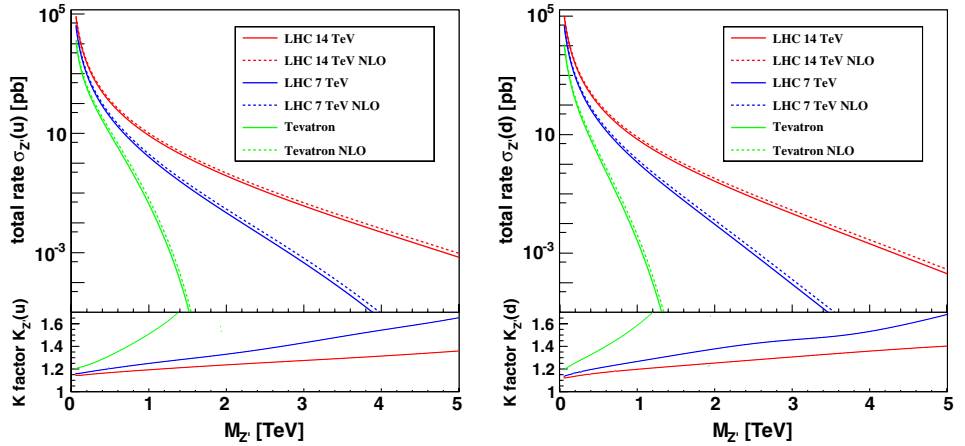

FIG. 2 (color online). Upper panel: the LO and NLO cross sections of $pp \to Z'$ process with a sequential couplings as a function of $m_{Z'}$ in hadron collision: (left) induced by up-type quark initial state, (right) induced by down-type quark initial state. Lower panel: the K factor as a function of $m_{Z'}$.

B. V' decay

In the $G(221)$ model the W' and Z' bosons can decay into SM fermions, gauge bosons, or a pair of SM gauge boson and Higgs boson. In this subsection we give detailed formula of partial decay widths of the extra gauge bosons.

First, consider the fermionic mode. The decay width of $V' \to \bar{f}_1 f_2$ is

$$\Gamma_{V'\to\bar{f}_1 f_2} = \frac{M_{V'}}{24\pi}\beta_0\Big[(g_L^2+g_R^2)\beta_1 + 6g_L g_R\frac{m_{f_1}m_{f_2}}{M_{V'}^2}\Big]\Theta(M_{V'}-m_{f_1}-m_{f_2}), \quad (18)$$

where

$$\beta_0 = \sqrt{1-2\frac{m_{f_1}^2+m_{f_2}^2}{M_{V'}^2}+\frac{(m_{f_1}^2-m_{f_2}^2)^2}{M_{V'}^4}}, \qquad \beta_1 = 1-\frac{m_{f_1}^2+m_{f_2}^2}{2M_{V'}^2}-\frac{(m_{f_1}^2-m_{f_2}^2)^2}{2M_{V'}^4}. \quad (19)$$

Note that the color factor is not included in Eq. (18) and the third generation quark decay channel opens only for a heavy Z' and W'.

Second, consider the bosonic decay mode, e.g., W' and Z' decay to gauge bosons and Higgs bosons. Such decay modes are induced by gauge interactions between the extra gauge boson and the SM gauge boson after symmetry breaking. Even though the couplings $g_{V'V_1V_2}$ and $g_{V'V_1H}$ are suppressed by the gauge boson mixing term $1/x$, the bosonic decay channel could be the major decay channel in certain models, e.g., fermiophobic model in which the extra gauge boson does not couple to fermions at all.

The decay width of $V' \to V_1 V_2$ is

$$\Gamma_{V'\to V_1V_2} = \frac{M_{V'}^5}{192\pi M_{V_1}^2 M_{V_2}^2}\times g_{V'V_1V_2}^2\beta_0^3\beta_1\Theta(M_{V'}-M_{V_1}-M_{V_2}), \quad (20)$$

where

$$\beta_0 = \sqrt{1-2\frac{M_{V_1}^2+M_{V_2}^2}{M_{V'}^2}+\frac{(M_{V_1}^2-M_{V_2}^2)^2}{M_{V'}^4}}, \qquad \beta_1 = 1+10\frac{M_{V1}^2+M_{V2}^2}{2M_{V'}^2}+\frac{M_{V_1}^4+10M_{V2}^2M_{V_2}^2+M_{V_1}^4}{M_{V'}^4}. \quad (21)$$

The width of $V' \to V_1 H$ (where $V_1 = W$ or Z boson and H is the lightest Higgs boson) is

$$\Gamma_{V'\to V_1H} = \frac{M_{V'}}{192\pi}\frac{g_{V'V_1H}^2}{M_{V_1}^2}\beta_0\beta_1\Theta(M_{V'}-M_{V_1}-M_{V_2}), \quad (22)$$

where

$$\beta_0 = \sqrt{1-2\frac{M_{V_1}^2+m_H^2}{M_{V'}^2}+\frac{(M_{V_1}^2-m_H^2)^2}{M_{V'}^4}}, \qquad \beta_1 = 1+\frac{10M_{V_1}^2-2m_H^2}{2M_{V'}^2}+\frac{(M_{V_1}^2-m_H^2)^2}{M_{V'}^4}. \quad (23)$$

The couplings $g_{V'V_1V_2}$ and $g_{V'V_1H}$ for various models are listed in Table II for reference. In this study, only left-handed neutrinos are considered while the possible right-handed neutrinos are assumed to be very heavy. In addition, we also assume all the heavy Higgs bosons, except the SM-like Higgs boson, decouple from the TeV scale. As a result, the total decay width of the W' boson is

$$\Gamma_{W',\mathrm{tot}} = 3\Gamma_{W'\to\bar{e}\nu}+2N_C\Gamma_{W'\to\bar{u}d}+N_C\Gamma_{W'\to\bar{t}b}+\Gamma_{W'\to WZ}+\Gamma_{W'\to WH}, \quad (24)$$

while the width of the Z' boson is

$$\Gamma_{Z',\mathrm{tot}} = 3\Gamma_{Z'\to\bar{e}e}+3\Gamma_{Z'\to\bar{\nu}\nu}+2N_C\Gamma_{Z'\to\bar{u}u}+3N_C\Gamma_{Z'\to\bar{d}d}+N_C\Gamma_{Z'\to\bar{t}t}+\Gamma_{Z'\to WW}+\Gamma_{Z'\to ZH}, \quad (25)$$

where $N_C = 3$ originates from summation of all possible color quantum number.

IV. INDIRECT AND DIRECT CONSTRAINTS

Even though the W' and Z' bosons are not observed yet, they could contribute to a few observables, which can be measured precisely at the low energy, via quantum effects. In this section, we perform a global-fit analysis of 37 EWPTs to derive the allowed model parameter space of those NP models of our interest. In addition, we also include direct search limits from the Tevatron and the LHC.

Note that $m_{W'}$ and $m_{Z'}$ are not independent in the $G(221)$ model; see Eqs. (3)–(5). In this study, we choose $M_{W'}$ as an input parameter. In addition, other independent parameters are the gauge mixing angle ϕ, and the mixing angle β in the electroweak symmetry breaking scale between two Higgs VEVs with $s_{2\beta} = \sin(2\beta)$ which only exists in BP-I. Our parameter scan is not sensitive to the parameter β as it contributes to physical observables only at the order of $1/x = v/u$. We then present our scan results in the plane of $(M_{W'}, c_\phi)$ or $(M_{W'}, M_{Z'})$.

A. Indirect search: electroweak precision tests

Constraints from the EWPTs [35,36] on the $G(221)$ model have been presented in our previous study [13]. Owing to the tree-level mixing between extra gauge bosons and SM gauge bosons in the $G(221)$ models, the conventional oblique parameters (S, T, U) cannot describe all the EWPT data. Therefore, a global fitting is in order. Our global analysis includes a set of 37 experiment observables, which is listed as follows:

(i) Z pole data (21): Z-boson total width Γ_Z, cross section $\sigma_{\rm had}$, ratios $R(f)$, LR, forward-backward, and charge asymmetries $A_{\rm LR}(f)$, $A_{\rm FB}(f)$, and $Q_{\rm FB}$;
(ii) $W^{\pm}$ and top data (3): W-boson mass M_W and total width Γ_W, and the top quark pole mass m_t;
(iii) νN-scattering (5): neutral current (NC) couplings $(g_{\rm L}^{\nu N})^2$ and $(g_{\rm R}^{\nu N})^2$, ratio of neutral current to charged current R_ν and $R_{\bar\nu}$;
(iv) νe^--scattering (2): NC couplings $g_V^{\nu e}$ and $g_A^{\nu e}$;
(v) Parity violation interactions (5): weak charge $Q_W(^{133}{\rm Cs})$, $Q_W(^{205}{\rm Tl})$, $Q_W(e)$, NC couplings C_1, C_2;
(vi) τ lifetime (1).

The number inside each set of parentheses denotes the number of the low energy precision observables. In our global χ^2 fitting, m_h and $\overline{m}_t$ (top quark mass in $\overline{\rm MS}$ scheme) are fixed as the best-fit value in the Standard Model prediction [13]. We use GAPP code [36] to find the best-fit values of the SM parameters. With constraint on Higgs mass $m_h > 115$ GeV from LEP II included, we obtain the best-fit values of the SM parameters[1]

$$m_h = 115 \text{ GeV}, \tag{26}$$

$$\bar{m}_t = 163.194 \text{ GeV}, \tag{27}$$

with the minimal χ^2:

$$\chi^2_{\rm min}/\text{d.o.f.} = 42.27/37. \tag{28}$$

In this work, we only present the contour of 95% confidence level in the plane of (x, c_ϕ) and refer readers to our previous paper for all the details.

B. Direct search at the tevatron and LHC

Another important bound on the $G(221)$ models originates from direct searches at the Tevatron and the LHC. Searches for the W' and Z' bosons as a s-channel resonance have been carried out at the Tevatron and LHC in leptonic decay modes, quark decay channels, and diboson decays. For the constraints from Tevatron, we use the latest Tevatron data:

(i) DØ: $p\bar{p} \to Z' \to e^+e^-$ ($\int \mathcal{L}dt = 5.4$ fb^{-1}) [39];
(ii) CDF: $p\bar{p} \to W'^{\pm} \to e\nu$ ($\int \mathcal{L}dt = 5.3$ fb^{-1}) [40];
(iii) CDF: $p\bar{p} \to W'^{\pm} \to t\bar{b}$ ($\int \mathcal{L}dt = 1.9$ fb^{-1}) [41];
(iv) CDF: $p\bar{p} \to Z' \to t\bar{t}$ ($\int \mathcal{L}dt = 955$ pb^{-1}) [42].

and LHC7 data:

(v) ATLAS: $pp \to W'^{\pm} \to \ell\nu$ ($\int \mathcal{L}dt = 1.04$ fb^{-1}) [19];
(vi) ATLAS: $pp \to Z' \to l^+l^-$ ($\int \mathcal{L}dt = 1.1$ fb^{-1}) [20];
(vii) CMS: $pp \to Z' \to t\bar{t}$ in the electron + jets channel ($\int \mathcal{L}dt = 4.33$ fb^{-1}) [43].

C. Parameter constraints

Using the result of all the indirect and direct searches mentioned above, we scan over the parameter space of several typical $G(221)$ models to locate allowed parameter contours at the 95% confidence level (CL). The NLO QCD correction to new heavy gauge boson production is included using the approach described in Sec. III. For each individual NP model, the total width is calculated with all the possible decay channels included, as discussed in Sec. III.

The parameter scan results are plotted in Figs. 3–5. In Fig. 5, the allowed region in SQD, TFD and UUD models are not shown because they are the same as ones in Fig. 4. In order to better understand the impact of various experiment data on the parameter space of the $G(221)$ model, we separate the indirect and direct search constraints into three categories: the electroweak indirect constraints (green region) and the direct search constraints from the Tevatron (red region) and the LHC7 (blue region). In Fig. 3, we note the following points:

(i) For LRD (LRT) model, LHC7 data has stronger constraint on W' and Z' masses than both EWPT and Tevatron constraints, and excludes the region where W' mass is smaller than 1.7 TeV (1.8 TeV) and Z' mass is smaller than 2.3 TeV (3.3 TeV);
(ii) for SQD model, although the W' and Z' with degenerate masses 500 GeV can be allowed by the EWPTs at large c_ϕ, the limits from Tevatron and LHC will exclude the region where W' and Z' masses are smaller than 1.5 TeV;
(iii) for all the models except the flavor universal models, such as LRD(T) and SQD, the EWPT data still hold the strongest constraints on the W' and Z' masses because of the nonuniversal flavor structure in these models;
(iv) in BP-I, with combined constraints, all the phobic models, in which the couplings of W' to either quarks or leptons are suppressed, can still have relatively light W' around 500 GeV, but heavier Z' (about 1.5 TeV);
(v) for the nonuniversal models, such as TFD and UUD, the electroweak indirect constraints are tighter than Tevatron and LHC7 direct search constraints, and push the new gauge boson mass up to more than 2 TeV (TFD) and 3 TeV (UUD), respectively.

In Figs. 4 and 5, we also want to point out:

(i) In BP-I, the $M_{W'} - c_\phi$ plane shows that small c_ϕ is favored by direct search constraints because the W'

[1]While submitting the paper to the journal, the ATLAS and CMS collaborations announced a 4.9σ and 5σ discovery of a SM-Higgs-boson-like resonance around 125 GeV in the $\gamma\gamma$ resonance [37,38]. The mass of the Higgs boson is chosen to be 115 GeV in this work. Our study is not sensitive to the Higgs boson mass, however. For example, changing the Higgs boson affects the W' decay width slightly such that all our results remain the same.

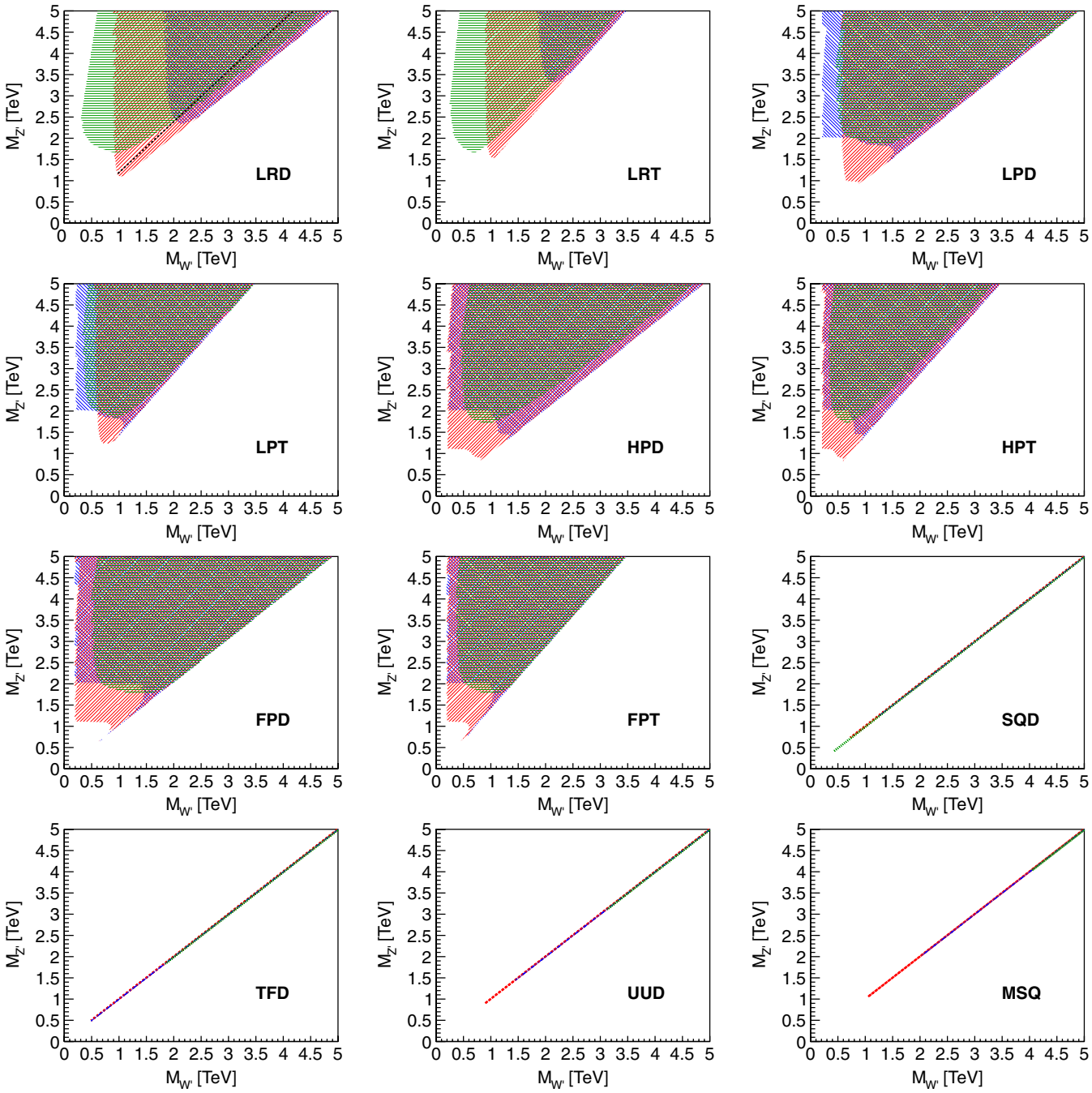

FIG. 3 (color online). Allowed parameter space (colored region) of the $G(221)$ model at 95% CL in the $M_{W'} - M_{Z'}$ plane after including indirect and direct constraints: EWPTs (green, vertical lines), Tevatron (red, top-right bottom-left diagonal lines), and LHC7 (blue, top-left bottom-right diagonal lines).

coupling is proportional to $1/s_\phi$, which leads to small W' production rate. However, in the $M_{Z'} - c_\phi$ plane, small c_ϕ is disfavored by direct search constraints because the mass relation $M_{Z'} \simeq M_{W'}/c_\phi$, pushing the exclusion region of small c_ϕ to larger $M_{Z'}$.

(ii) In BP-II, the shapes in the small c_ϕ region are very similar because the production cross section of W' and Z' is proportional to $\tan\phi$ in all models such as SQD, TFD, and UUD. Because quarks and leptons are ununified in UUD, the gauge couplings to leptons are proportional to $\cot\phi$, which implies the large c_ϕ region is also disfavored.

(iii) Within the direct searches, for LRD(T), the most sensitive constraint comes from W' leptonic decay channel, while for phobic models, the tightest constraints comes from Z' leptonic decay channel. This

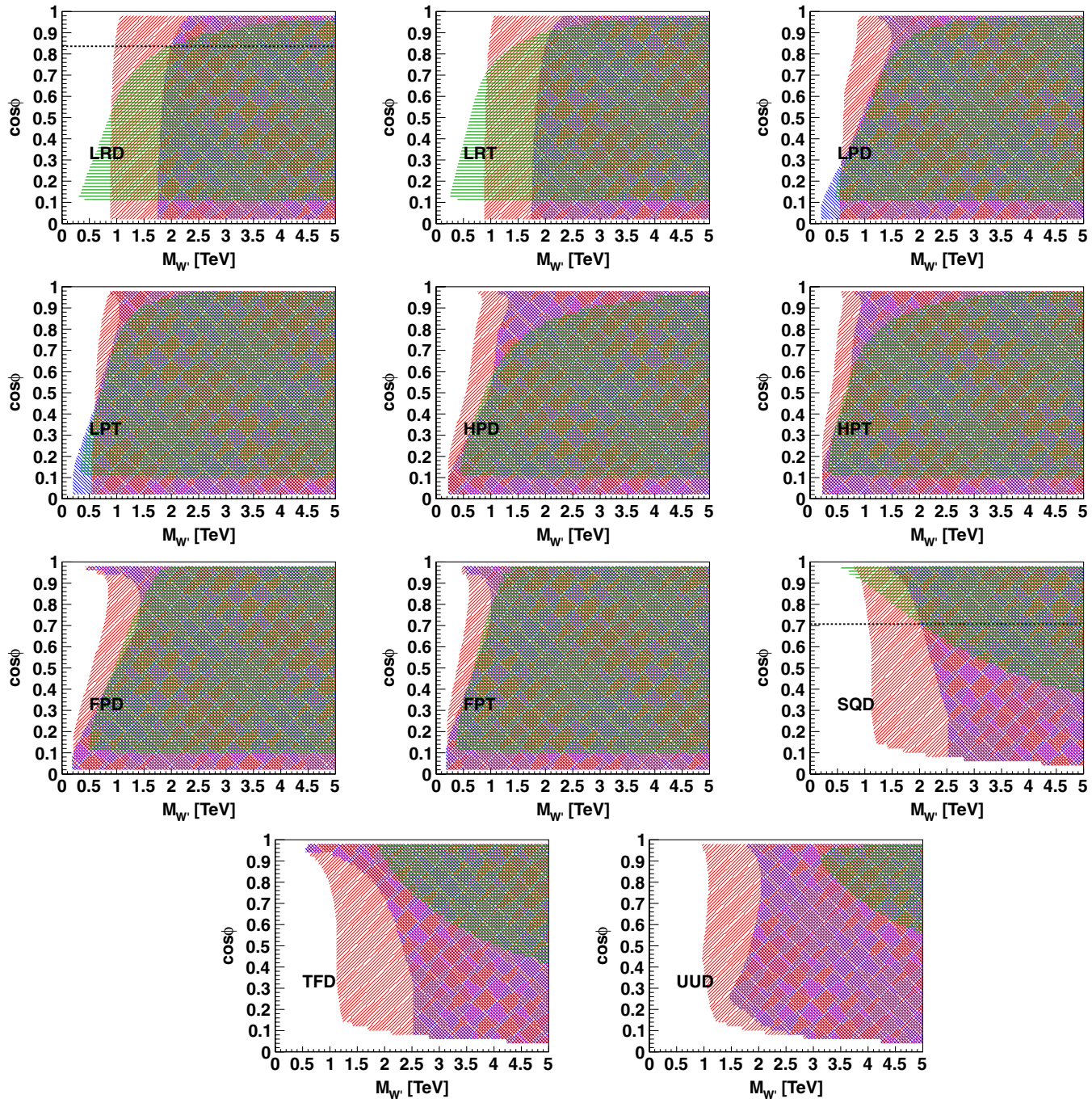

FIG. 4 (color online). Allowed parameter space (colored region) of the $G(221)$ model at the 95% CL in the $M_{W'} - c_\phi$ plane after including indirect and direct search constraints: EWPTs (green, vertical lines), Tevatron (red, top-right bottom-left diagonal lines), and LHC7 (blue, top-left bottom-right diagonal lines). The dashed black lines in LRD and SQD represent MLR and MSQ models.

explains that the contours in the phobic models have similar shapes, but different from those in the LRD(T) models.

D. V' decay width

Figures 6 and 7 show the largest total decay widths of W' and Z' on the parameter space of $G(221)$ models, where we have considered the constraint from low energy precision data, LEP, Tevatron, and LHC7 data. We can see that the ratio of total width with respect to the relevant mass is a few percent in most regions of parameter space. The ratio of total decay width to mass can reach at most 10% only in some edge regions of parameter space. Therefore, the narrow width approximation in our study is valid.

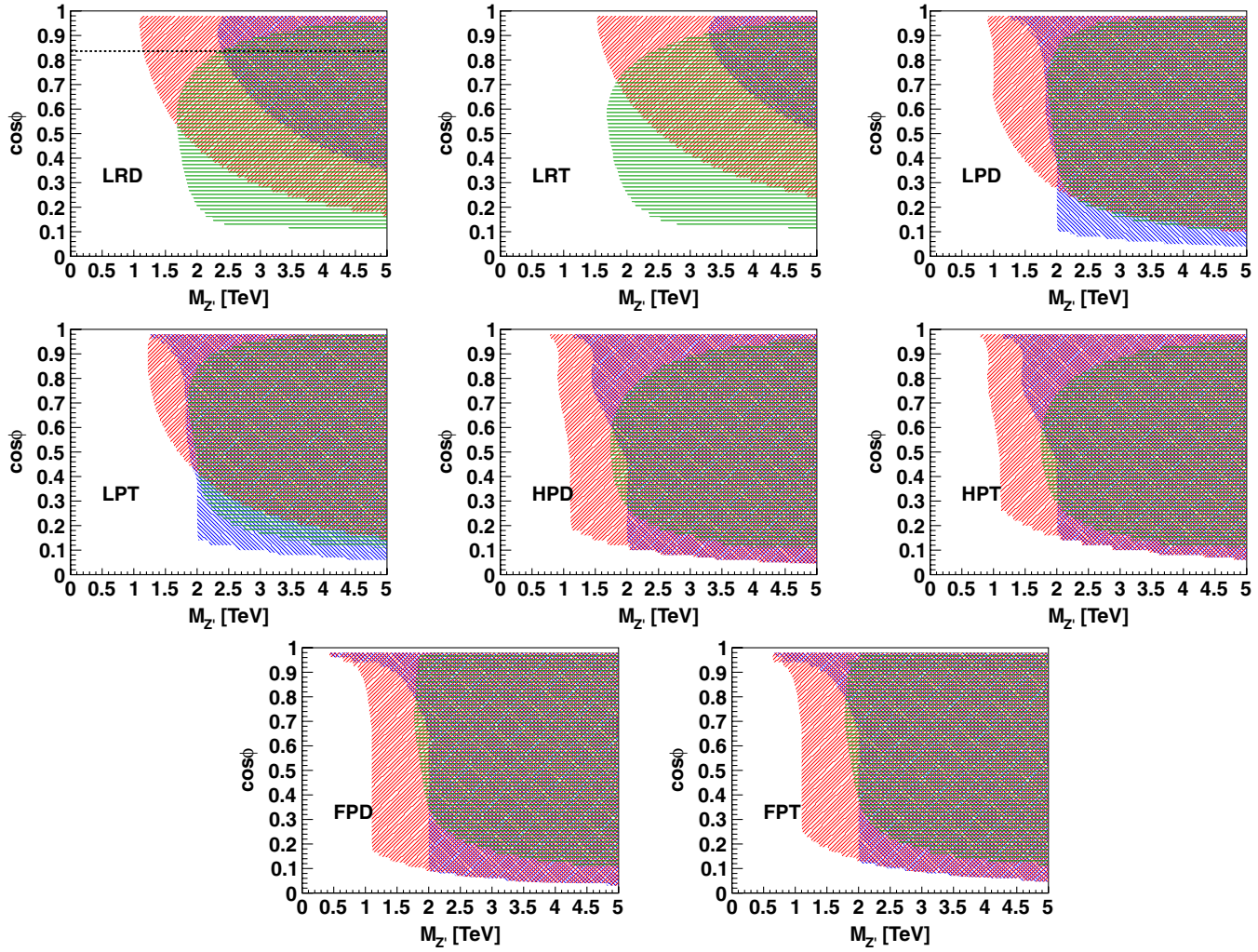

FIG. 5 (color online). Allowed parameter space (colored region) of the $G(221)$ model at 95% CL in the $M_{W'} - c_\phi$ plane after including indirect and direct search constraints: EWPTs (green, vertical lines), Tevatron (red, top-right bottom-left diagonal lines), and LHC7 (blue, top-left bottom-right diagonal lines). The dashed black lines in LRD represent MLR models.

Besides, by comparing Figs. 6 and 7, we can see for the phobic models the Z' width is much larger than the W' width, which is usually below 10 GeV.

V. LHC DISCOVERY POTENTIAL AND SIGNATURE SPACE

In early LHC7 results, the combined constraints from current direct searches and indirect EWPTs play a crucial role in specifying the unexplored parameter space. Given the allowed parameter space discussed in the previous sections, we are able to provide the following information:

(i) the integrated luminosity, with which the LHC can discover the W' and/or Z' for certain mass in various $G(221)$ models;

(ii) the region of parameter space that could be accessed for different luminosities and energies in the LHC run;

(iii) the possibility to identify NP models in our classification, once the W' and/or Z' are discovered.

To be specific, we consider two different scenarios: an early run with $\sqrt{s} = 7$ TeV and an integrated luminosity of 5.61 fb^{-1} (the maximal integrated luminosity reached at the 7 TeV); a long run with $\sqrt{s} = 14$ TeV and $\mathcal{O}(10^3)$ fb^{-1} integrated luminosity.

To get the expected luminosity contour, one has to calculate the signal and background cross sections at LHC7 and LHC14 for each point in the parameter space of the models. In principle, the complete Monte Carlo simulations for the signal and background including efficiency analysis in the $G(221)$ models have to be used to obtain the needed luminosity for the discovery or exclusion at 7 TeV and 14 TeV. However, in the Drell-Yan production process, all the model-independent effects, including the kinematic cuts, can be factorized out from the model-dependent part, which only depends on the gauge couplings and branching ratios, as shown in Sec. II. Therefore, the simulation on one benchmark model, such as the sequential W' and Z' model, can

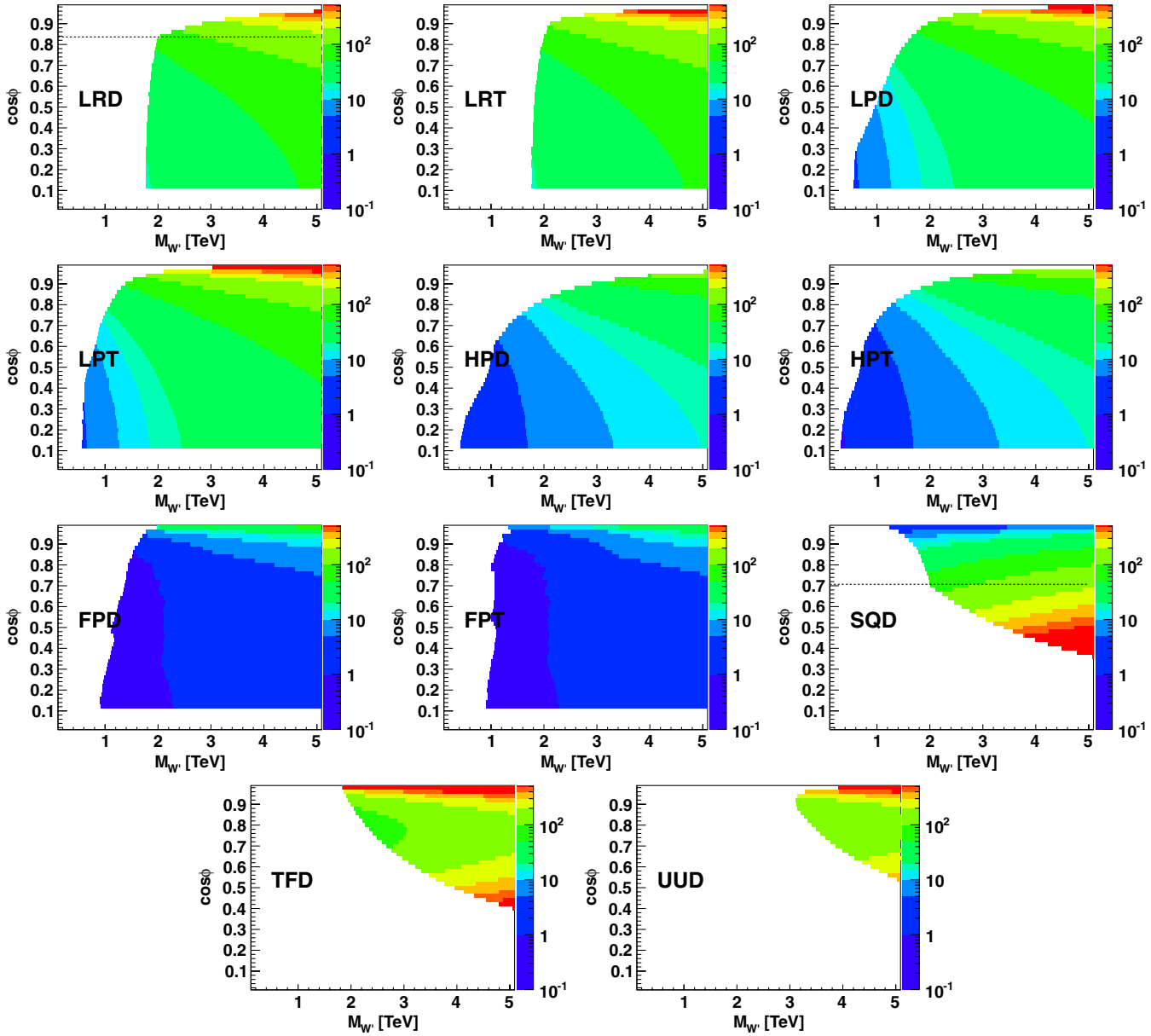

FIG. 6 (color online). The largest total decay widths (GeV) of W' in the $M_{W'} - c_\phi$ plane for different $G(221)$ models within the allowed parameter space constrained by current experiment data. The color palette shows the largest total decay widths in unit GeV.

provide the needed luminosity information for the other models. At the LHC7, the complete simulation on the signal and backgrounds including detection efficiency has been done in Refs. [19,20]. At the LHC14, the ATLAS TDR [44] have done the detailed studies on the discovery potentials for the sequential W' and Z' model. The luminosity needed for other new physics models can be obtained by properly scaling the luminosity obtained for the sequential model.

Here, we summarize the event analysis procedures at the current LHC and in the ATLAS TDR. At the LHC7, we adopt the ATLAS simulation and analysis with integrated luminosity at about 1 fb^{-1}. Both electron and muon channels are considered in both W' and Z' searches. For the W' searches, the missing energy in both channels is required to be above the threshold energy of 25 GeV. Furthermore, the cut on the transverse mass of the lepton and missing energy system varies as the W' mass increases. For more detailed information, please refer to Refs. [19,20]. In the ATLAS TDR, for the sequential W', the simulation on the lepton plus missing transverse energy signal at high mass region is performed. We list the event selection and cut-based analysis as follows:

(i) Events are required to have exactly one reconstructed lepton with $p_T > 50$ GeV within $|\eta| < 0.25$, and isolated from jets with $\Delta R_{\ell j} = 0.5$;

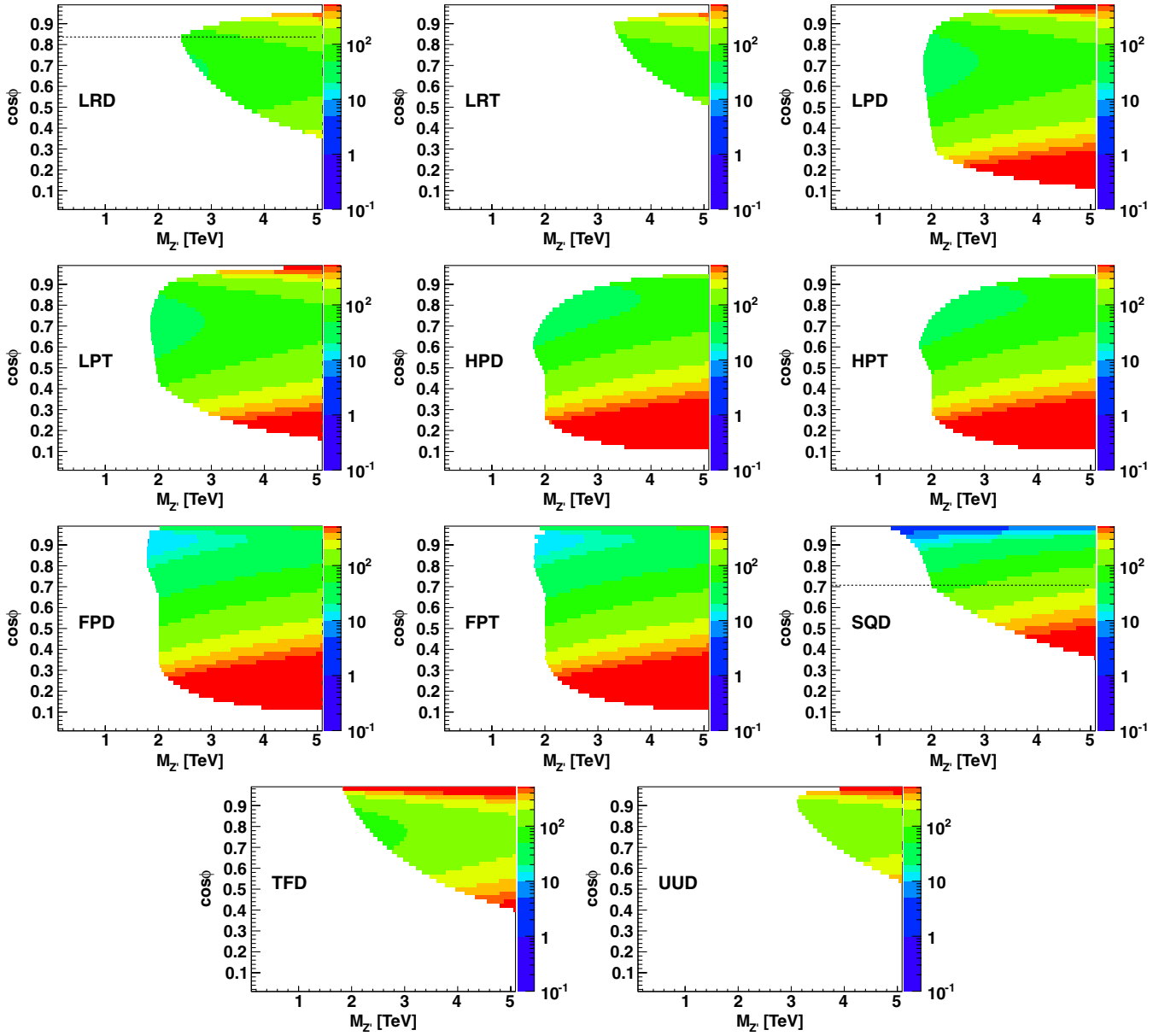

FIG. 7 (color online). The largest total decay widths (GeV) of Z' in the $M_{Z'} - c_\phi$ plane for different $G(221)$ models within the allowed parameter space constrained by current experiment data. The color palette shows the largest decay total widths in unit GeV.

(ii) the lepton reconstruction is smeared by $\sigma(1/p_T) = 0.011/p_T \otimes 0.00017$, while the jet resolution is taken as $\sigma(E_T) = 0.45 \times \sqrt{E_T} \otimes 5\%$;
(iii) missing transverse energy $E_T^{\rm mis} > 50$ GeV;
(iv) to reduce the dijet and $t\bar{t}$ backgrounds, a lepton fraction is required to be $\sum p_T/(\sum p_T + \sum E_T) > 0.5$;
(v) transverse mass $m_T = \sqrt{2p_T E_T^{\rm mis}(1 - \cos\Delta\phi)} > 0.7 \times M_{W'}$, where $\Delta\phi$ is the angle between the momentum of the lepton and the missing momentum.

For the sequential Z', we list the event selection and analysis on the dilepton final states as follows:

(i) Events are required to have exactly two reconstructed same-flavor opposite-charged leptons with at least one lepton $p_T > 30$ GeV, within $|\eta| < 0.25$;
(ii) dilepton invariant mass window $|m_{\ell\ell} - M_{Z'}| < 4 \times \Gamma_{Z'}$.

Next, we explore the LHC sensitivity to W' and Z' bosons. We can quantify the sensitivity to new physics discovery or set exclusion limits on it based on statistics. Specifically, for the case of discovery, we would like to know the statistical significance (S) for discovery, which characterizes the inconsistency of the experiment data with a background-only hypothesis. If there is no discovery at a given luminosity, we set exclusion limits on new physics.

In the counting experiments, suppose one has an experiment which counts n events, modeled as a Poisson distribution with mean $s + b$, where s is the expected signal rate, and b is the expected background rate. The probability of measuring n events is therefore

$$P(n|s, b) = \frac{(s + b)^n}{n!} e^{-(s+b)}. \tag{29}$$

Using a profile likelihood ratio as the test statistic, the expected significance is obtained as follows [45]:

$$S = \sqrt{2((s + b)\ln(1 + s/b) - s)}. \tag{30}$$

For sufficiently large b, we can expand the logarithm in s/b and obtain the widely used significance

$$S = \frac{s}{\sqrt{b}}(1 + \mathcal{O}(s/b)). \tag{31}$$

In addition to establishing discovery by rejecting the background hypothesis, we can consider the signal hypothesis as well. It is common to use CL α and the related p value to quantify the level of incompatibility of data with a signal hypothesis. The profile likelihood ratio q_μ is used as the test statistic [45]. For a sufficiently large data sample, the probability density of q_μ takes on a well-defined χ^2 distribution with mean $\hat{\mu}$ and variance $\hat{\sigma}$ for one degree of freedom. Given the p value for each number of signal events s, we can obtain the upper limit $s^{\rm up}$ on the number of signal events,

$$s^{\rm up} = \hat{\mu} + \hat{\sigma}\Phi^{-1}(1 - \alpha), \tag{32}$$

where the mean and variance of the χ^2 distribution are $\hat{\mu} = n - b$, and $\hat{\sigma} = \sqrt{b}$ for large data sample, and Φ is the cumulative distribution of the standard Gaussian with zero mean and unit variance. For the expected upper limit, in which the data count is taken as the background sum, the upper limit at confidence level $\alpha = 95\%$ is

$$s^{\rm up} = \Phi^{-1}(0.05) \cdot \sqrt{b} = 1.64 \times \sqrt{b}. \tag{33}$$

So for a sufficiently large data sample, the equivalent significance Z for excluding a signal hypothesis is given by

$$Z = \frac{s^{\rm up}}{\sqrt{b}} = 1.64. \tag{34}$$

For instance, when expressing the significance for 5σ discovery with the exclusion upper limit at the 95% CL, a factor $S/Z = 5/1.64 \simeq 3$ needs to be applied.

Denoting by σ_s (σ_b) the inclusive cross section of the signal (background), ϵ_s (ϵ_b) the cut acceptance of the signal (background), and $\mathcal{L}$ the integrated luminosity, the number of signal (background) events can be written as

$$s = \sigma_s \epsilon_s \mathcal{L}, \tag{35}$$

$$b = \sigma_b \epsilon_b \mathcal{L}. \tag{36}$$

For a sufficiently large data sample, both S and Z have a scaling behavior with the integrated luminosity,

$$S \simeq Z \simeq \frac{s}{\sqrt{b}} = \frac{\sigma_s \epsilon_s}{\sqrt{\sigma_b \epsilon_b}} \times \sqrt{\mathcal{L}}. \tag{37}$$

Figure 8 displays the 5σ discovery potential (fb^{-1}) for LHC7 via W' leptonic decay channel, and current combined constraints are within the solid black contour. The LRD(T) and MLR models can be further constrained when the integrated luminosity for LHC7 reaches its maximum 5.6 fb^{-1}. However, the other models need much more luminosity, which even exceeds the total integrated luminosity (5.6 fb^{-1}) at LHC7. Therefore, the W' leptonic decay channel cannot make further contributions to discovering these $G(221)$ models, except for some small region in LRD(T) and MLR. In Fig. 3, it shows that the EWPTs constraints are stronger than those from the Tevatron and the LHC7, except LRD(T) and MLR. This means that compared to EWPTs, the LHC7 direct search via the W' leptonic decay channel for the new physics models with $G(221)$ gauge group structure can put further constraint only on LRD(T) and MLR. For the other models, the direct search at LHC7 for s-channel W' production with leptonic decay cannot compete with seeking for deviation from SM predictions via EWPTs.

Figure 9 shows the 5σ discovery potential (fb^{-1}) at the LHC7 via the Z' leptonic decay channel, and the current combined constraints are within the solid black contour. We can see that for LRD(T), SQD, TFD, UUD, MLR, and MSQ, further discovery via the Z' leptonic decay channel needs more than 100 fb^{-1}, which is definitely far beyond the total integrated luminosity before LHC switches away from 7 TeV. However, some corner of the parameter space of LPD(T), HPD(T), and FPD(T) can be further tested when LHC7 reaches 5.6 fb^{-1}. Especially, for HPD(T) and FPD(T), there are small regions where Z' can be discovered with a few fb^{-1} luminosity, or these parameters can be excluded with less than one fb^{-1} luminosity. At the LHC7, the Z' leptonic decay channel is more efficient than EWPTs on discovering LPD(T), HPD(T), and FPD(T). For LRD(T), LPD(T), and HPD(T), EWPTs are more sensitive to the large c_ϕ region, where LHC7 cannot compete with EWPTs. For SQD, TFD, and UUD, both W' and Z' leptonic decay channels cannot make further tests at LHC7, because the constraint from EWPTs for UUD is much stronger than Tevatron or LHC7 data, as shown in Fig. 3.

Figure 10 presents the 5σ discovery potential (fb^{-1}) at the LHC14 via the W' leptonic decay channel, and current constraints are within the solid black contour. After the LHC14 collects 10 fb^{-1}, a sizable region of parameter space will be further tested, except all the phobic models, LPD(T), HPD(T), and FPD(T). For the phobic models, a very large integrated luminosity is needed to have 5σ discovery because of the small total cross section in the W' leptonic decay channel, which is either suppressed by the production rate of the W', such as HPD(T) and FPD(T), or suppressed by the decay branching ratio, such as LPD (T) and FPD(T). With a 10 fb^{-1} luminosity, for LRD(T),

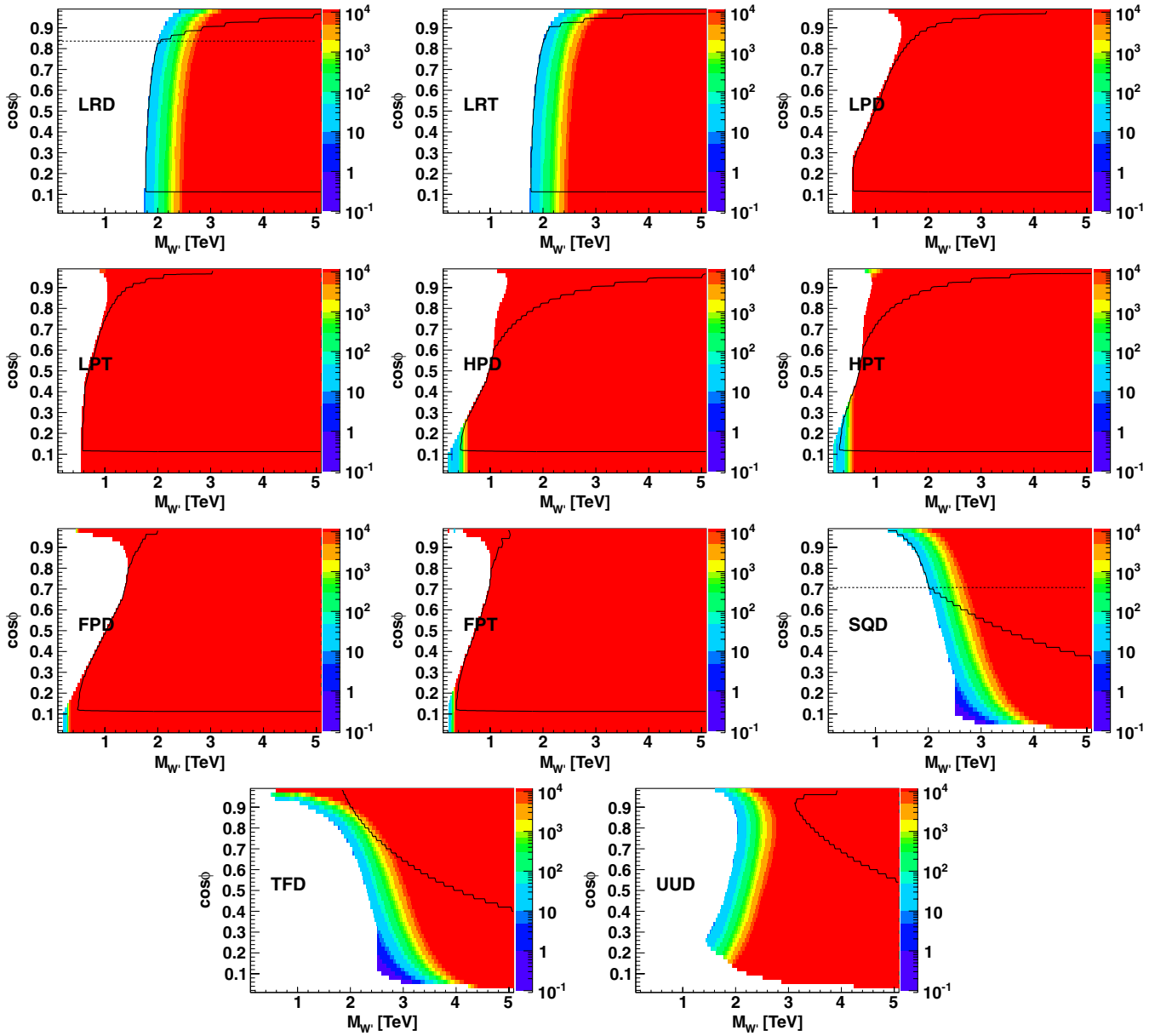

FIG. 8 (color online). 5σ Discovery potential (fb^{-1}) for different luminosity at LHC7 via W' leptonic decay channel. The color palette shows the integrated luminosity with unit fb^{-1}. EWPT constraints are within solid black contour.

the discovery potential for W' mass can reach more than 3 TeV, and the W' mass discovery for MLR can reach more than 4 TeV. Furthermore, for the large c_ϕ region in LRD (T), the LHC14 search via W' leptonic decay channel can easily probe the large $M_{W'}$ region with several fb^{-1}. In BP-II, the current constraints already pushed the W' to the large mass region. However, with a 10 fb^{-1} integrated luminosity, for SQD, TFD, and UUD models, most of the allowed region below 5 TeV W' mass can be further tested. For relatively small c_ϕ in SQD and TFD, a few fb^{-1} luminosity can even probe W' boson beyond 5 TeV. When the LHC is upgraded to 14 TeV, SQD, TFD, and UUD can be further tested, exploring the region where current constraints cannot reach. This shows that the capability of LHC14 is far beyond LHC7. However, none of the lepton phobic models, such as LPD(T), HPD(T), and FPD(T), can be tested at the LHC with 14 TeV, if only the leptonic decay channel of the W' boson is considered.

Figure 11 shows the 5σ discovery potential (fb^{-1}) for the LHC14 via the Z' leptonic decay channel, and current combined constraints are within the solid black contour. For the models other than LRD(T), UUD, and MLR, the LHC14 can already test the parameter space effectively with the integrated luminosity less than 1 fb^{-1}. However, for the FPD(T), SQD, and TFD models, EWPTs are more sensitive to the large c_ϕ region. Also, if the luminosity can reach 10 fb^{-1}, we can test a large parameter space region, where we can either discover new physics based on these

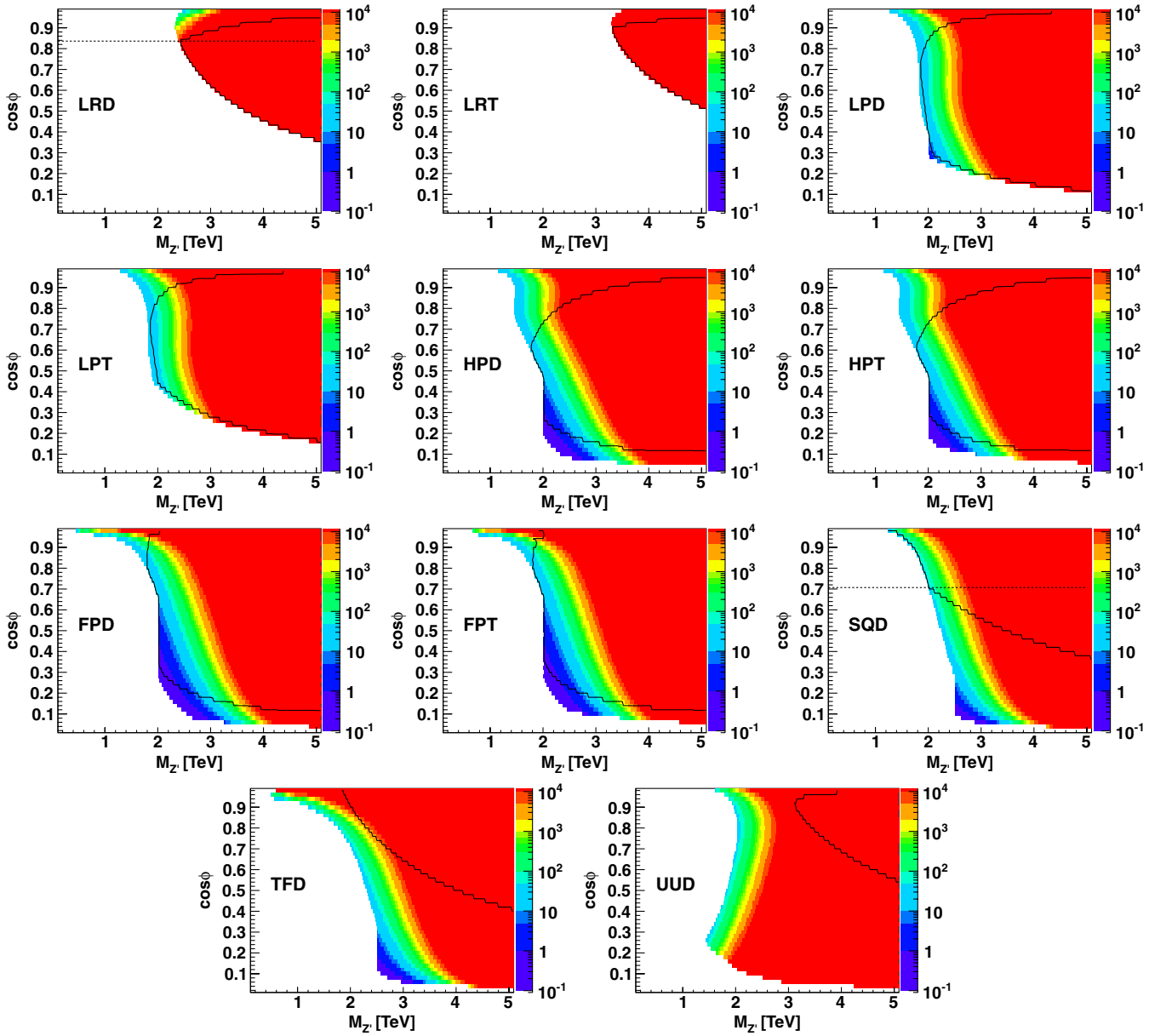

FIG. 9 (color online). 5σ Discovery potential (fb^{-1}) for different luminosity at LHC7 via Z' leptonic decay channel. The current combined constraints are within the solid black contour. The color palette shows the integrated luminosity with unit fb^{-1}. The dashed black lines in LRD and SQD represent MLR and MSQ models.

models or constrain the parameters in the relevant region. For LRD(T), UUD, and MLR, when integrated luminosity is accumulated to more than 100 fb^{-1}, LHC14 data can have sizeable parameter space further tested up to even beyond 5 TeV $M_{Z'}$. For LRD(T), the Z' leptonic decay channel is less effective than the W' channel. However, for the phobic models, such as LPD(T), FPD(T), and HPD(T), there is no $\mathcal{O}(1/x)$ suppression on the couplings of Z' to fermions, unlike the couplings of W' to fermions. So the Z' leptonic decay channel is much more effective than W' for the investigation based on the LHC14 data. Especially, for the small c_ϕ region, a few pb^{-1} luminosity can probe very large $M_{Z'}$. In the phobic models, observing a Z' alone cannot rule out the possibility of non-Abelian gauge extension of new physics.

In BP-II, both Z' and W' leptonic decay channels are suitable to explore the allowed parameter space of the models. Since the mass of W' and Z' are degenerate in BP-II, discovering degenerated W' and Z' in the leptonic decay channels at the same time will be the distinct feature compared to the models in BP-I. Compared to the LHC7 discovery potentials in Figs. 8–11 show that for LHC, the upgrade of the center-of-mass energy from 7 TeV to 14 TeV is much more efficient than accumulation of luminosity. For instance, for FPD(T), the Z' leptonic decay

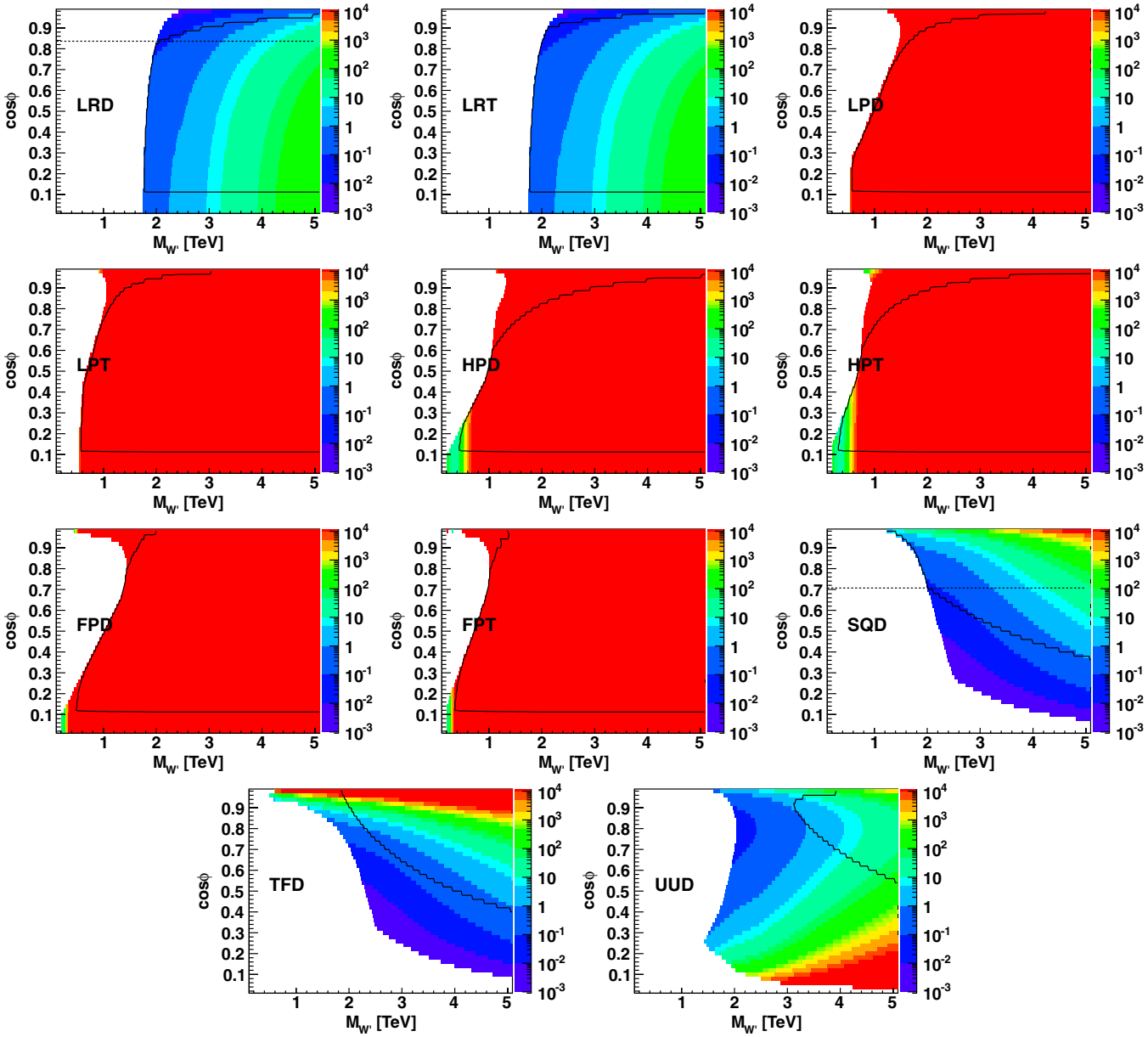

FIG. 10 (color online). 5σ Discovery potential (fb^{-1}) for different luminosity at LHC14 via W' leptonic decay channel. The color palette shows the integrated luminosity with unit fb^{-1}. The current constraints are within solid black contour. The dashed black lines in LRD and SQD represent MLR and MSQ models.

channel at LHC14 with less than 1 fb^{-1} can explore some region of parameter space, while LHC7 needs more than 10^4 fb^{-1} luminosity to achieve the similar sensitivity. For all these $G(221)$ models, LHC14 can exceed the capability of current combined constraints and have promising discovery potential.

If the heavy gauge bosons W' and/or Z' are not discovered, the potential for discovery can be converted to the 95% CL exclusion limits on the heavy gauge bosons W' and/or Z' using the relations $Z = S/3$ as discussed above. Equivalently, the luminosity for exclusion limits is about one order of magnitude lower than the discovery luminosity. Therefore, as shown in Fig. 8, supposing on signals found, via W' leptonic decay channel, W' mass in LRD(T) can be further excluded by about 100 GeV after the LHC7 collects 5.61 fb^{-1} luminosity. Figure 9 shows that via Z' leptonic decay channel, one can expect slightly further exclusion on LPD(T), HPD(T), and FPD(T) at LHC7. At the LHC14, as shown in Figs. 10 and 11, the exclusion region can extend very fast when luminosity is accumulated. For instance, via W' leptonic decay channel, 1 fb^{-1} can exclude most of the parameter region for LRD(T), SQD, TFD, and UUD, and 10 fb^{-1} can completely remove the possibility of $M_{Z'}$ less than 5 TeV in these models if there is no any sign of W' production. For LPD(T), HPD (T), and FPD(T), Z' leptonic decay channel at the LHC14

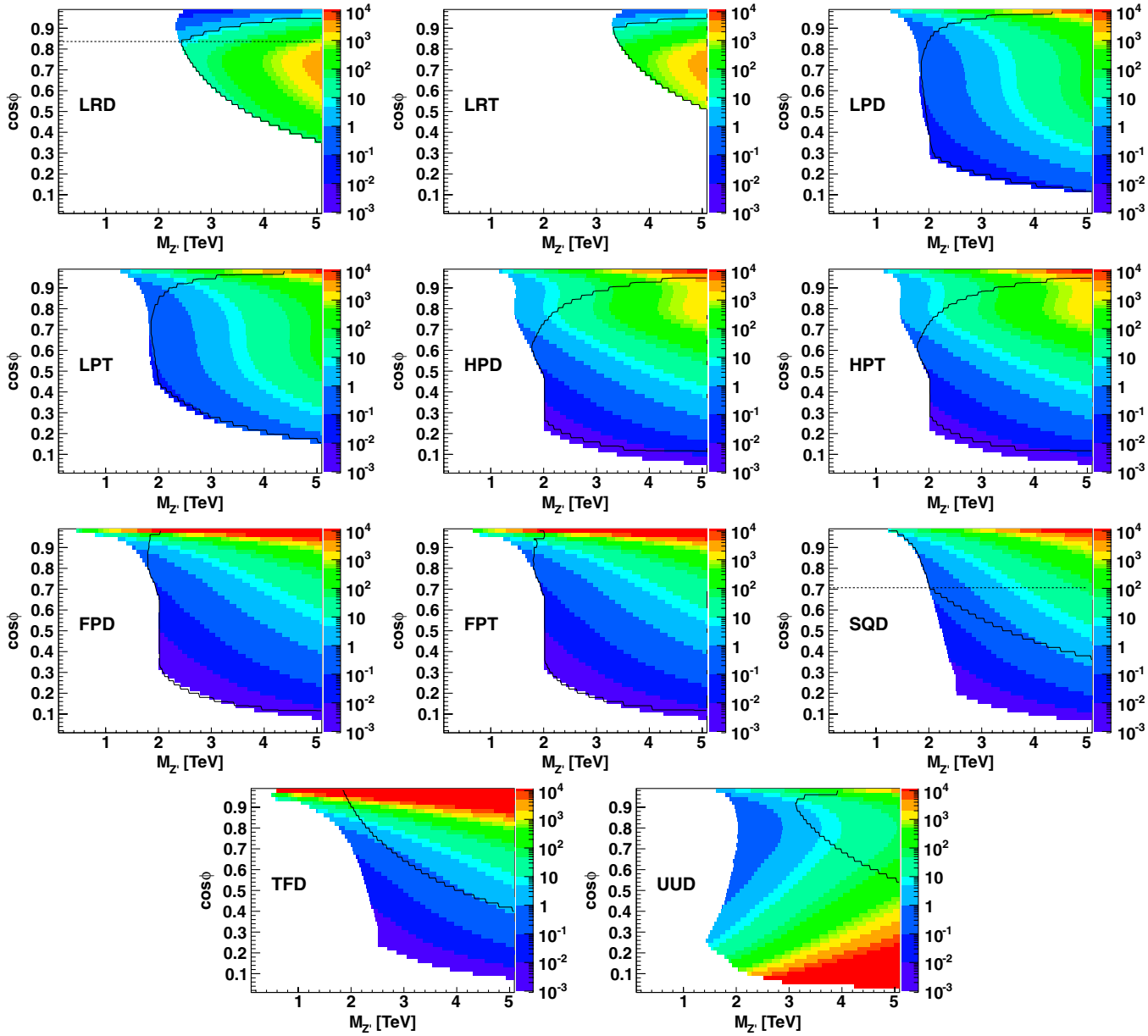

FIG. 11 (color online). 5σ Discovery potential (fb^{-1}) for different luminosity at LHC14 via Z' leptonic decay channel. The color palette shows the integrated luminosity with unit fb^{-1}. The current combined constraint are within solid black contour. The dashed black lines in LRD and SQD represent MLR and MSQ models.

can be used to exclude most of the parameter space region with only 1 fb^{-1} luminosity. Then, data with 10 fb^{-1} luminosity at LHC14 may leave LPD(T) and HPD(T) and FPD(T) only a corner of parameter space at large c_ϕ to survive. The shapes of the exclusion contours are the same as these at the discovery contours.

VI. CONCLUSION

In this paper, we have discussed the potential for discovering, or setting limits on, the extra heavy gauge bosons W' and/or Z' using two different scenarios at the LHC: an early run with $\sqrt{s} = 7$ TeV and total integrated luminosity of 5.61 fb^{-1} and a long run with $\sqrt{s} = 14$ TeV and 100 fb^{-1} integrated luminosity. The EWPTs, Tevatron, and LHC data have been used to set bounds on the allowed parameter space. We showed that direct searches give tighter bounds than EWPTs in BP-I. Although LHC data surpass the constraint from Tevatron and EWPTs constraints in LRD and LRT models, in other models, the parameter space depends nontrivially on the present bounds, especially during the early LHC runs. The unexplored parameter space will become accessible for 5σ discovery at different time scales. In LRD(T), it is more efficient to use the W' leptonic decay channel for discovery or exclusion than the Z' leptonic decay channel. In the

TABLE III. The current lowest limits and discovery reaches at the LHC14 with 100 fb^{-1} luminosity on W' and Z' masses.

Models	Current $M_{W'}$ Limit (TeV)	$M_{W'}$ LHC14 Reach (TeV)	Current $M_{Z'}$ Limit (TeV)	$M_{Z'}$ LHC14 Reach (TeV)
LRD (LRT)	1.72 (1.76)	3.2–5	2.25 (3.2)	2.8–5
LPD (LPT)	0.55 (0.55)	No improvement	1.8 (1.8)	3.5–5
HPD (HPT)	0.46 (0.35)	0.55	1.7 (1.7)	3–5
FPD (FPT)	0.5 (0.4)	No improvement	1.75 (1.75)	1.75–5
SQD	1.25	3.5–5	1.25	1.5–5
TFD	1.7	2–5	1.7	2–5
UUD	3.1	4–5	3.1	3.3–5

phobic models, it is challenging to discover a W' decaying into the leptonic mode. Hence, observing a Z' alone cannot rule out the possibility of NP models with non-Abelian gauge extension of the Standard Model. In BP-II models, both the Z' and W' leptonic decay channel are suitable to explore the allowed parameter space. Discovering degenerate W' and Z' in the leptonic decay channels at the same time will be the distinct feature in BP-II. In Table III, we summarize the current constraints and LHC14 reaches with 100 fb^{-1} luminosity on the W' and Z' masses in various models. If one needs to identify new physics models more precisely, one has to combine different discovery channels, such as top quark pair, single top quark production for the heavy resonances, or study angular distributions, or other properly defined asymmetries, in the most promising regions of parameter space of the models considered. For example, the LPD(T), HPD(T), and FPD(T) models can be further explored by examining the single-top production, the associate production of W' and W (or Z) bosons, and the production of weak gauge boson pairs from electroweak gauge boson fusion processes.

ACKNOWLEDGMENTS

We thank Wade Fisher for discussing the LHC results on putting limits on the W' mass. We thanks Reinhard Schwienhorst for his comments on part of this draft. The work of Z. L., J. H. Y. and C. P. Y. was supported by the U.S. National Science Foundation under Grant No. PHY-0855561. Q. H. C. was supported in part by the National Natural Science Foundation of China under Grant No. 11245003.

[1] R. Mohapatra and J. C. Pati, Phys. Rev. D **11**, 2558 (1975).
[2] R. N. Mohapatra and J. C. Pati, Phys. Rev. D **11**, 566 (1975).
[3] G. Senjanovic and R. N. Mohapatra, Phys. Rev. D **12**, 1502 (1975).
[4] R. N. Mohapatra and G. Senjanovic, Phys. Rev. D **23**, 165 (1981).
[5] R. S. Chivukula, B. Coleppa, S. Chiara, E. Simmons, H.-J. He, M. Kurachi, and M. Tanabashi, Phys. Rev. D **74**, 075011 (2006).
[6] V. D. Barger, W.-Y. Keung, and E. Ma, Phys. Rev. D **22**, 727 (1980).
[7] V. D. Barger, W.-Y. Keung, and E. Ma, Phys. Rev. Lett. **44**, 1169 (1980).
[8] H. Georgi, E. E. Jenkins, and E. H. Simmons, Phys. Rev. Lett. **62**, 2789 (1989).
[9] H. Georgi, E. E. Jenkins, and E. H. Simmons, Nucl. Phys. **B331**, 541 (1990).
[10] X. Li and E. Ma, Phys. Rev. Lett. **47**, 1788 (1981).
[11] E. Malkawi, T. M. Tait, and C. Yuan, Phys. Lett. B **385**, 304 (1996).
[12] X.-G. He and G. Valencia, Phys. Rev. D **66**, 013004 (2002).
[13] K. Hsieh, K. Schmitz, J.-H. Yu, and C.-P. Yuan, Phys. Rev. D **82**, 035011 (2010).
[14] T. G. Rizzo, in *Proceedings of Theoretical Advanced Summer Institute TASI-2006*, edited by S. Dawson and R. N. Mohapatra (World Scientific, Hackensack, 2008).
[15] E. L. Berger, Q.-H. Cao, C.-R. Chen, and H. Zhang, Phys. Rev. D **83**, 114026 (2011).
[16] C. W. Bauer, Z. Ligeti, M. Schmaltz, J. Thaler, and D. G. Walker, Phys. Lett. B **690**, 280 (2010).
[17] V. Khachatryan *et al.* (CMS Collaboration), Phys. Lett. B **698**, 21 (2011).
[18] S. Chatrchyan *et al.* (CMS Collaboration), J. High Energy Phys. 05 (2011) 093.
[19] G. Aad *et al.* (ATLAS Collaboration), Phys. Lett. B **705**, 28 (2011).
[20] G. Aad *et al.* (ATLAS Collaboration), Phys. Rev. Lett. **107**, 272002 (2011).
[21] P. Langacker, Rev. Mod. Phys. **81**, 1199 (2009).
[22] M. S. Carena, A. Daleo, B. A. Dobrescu, and T. M. Tait, Phys. Rev. D **70**, 093009 (2004).
[23] E. Salvioni, G. Villadoro, and F. Zwirner, J. High Energy Phys. 11 (2009) 068.
[24] E. Accomando, A. Belyaev, L. Fedeli, S. F. King, and C. Shepherd-Themistocleous, Phys. Rev. D **83**, 075012 (2011).

[25] K. R. Lynch, E. H. Simmons, M. Narain, and S. Mrenna, Phys. Rev. D **63**, 035006 (2001).
[26] M. Schmaltz and C. Spethmann, J. High Energy Phys. 07 (2011) 046.
[27] A. Maiezza, M. Nemevsek, F. Nesti, and G. Senjanovic, Phys. Rev. D **82**, 055022 (2010).
[28] C. Grojean, E. Salvioni, and R. Torre, J. High Energy Phys. 07 (2011) 002.
[29] M. Nemevsek, F. Nesti, G. Senjanovic, and Y. Zhang, Phys. Rev. D **83**, 115014 (2011).
[30] R. Torre, arXiv:1109.0890.
[31] T. Jezo, M. Klasen, and I. Schienbein, Phys. Rev. D **86**, 035005 (2012).
[32] W.-Y. Keung and G. Senjanovic, Phys. Rev. Lett. **50**, 1427 (1983).
[33] E. L. Berger, Q.-H. Cao, J.-H. Yu, and C.-P. Yuan, Phys. Rev. D **84**, 095026 (2011).
[34] P. M. Nadolsky, H.-L. Lai, Q.-H. Cao, J. Huston, J. Pumplin, D. Stump, W.-K. Tung, and C.-P. Yuan, Phys. Rev. D **78**, 013004 (2008).
[35] C. Amsler *et al.* (Particle Data Group), Phys. Lett. B **667**, 1 (2008).
[36] J. Erler, arXiv:hep-ph/0005084.
[37] ATLAS Collaboration, Report No. ATLAS-CONF-2012-093 (2012).
[38] CMS Collaboration, Report No. CMS-PAS-HIG-12-020 (2012).
[39] V. M. Abazov *et al.* (D0 Collaboration), Phys. Lett. B **695**, 88 (2011).
[40] T. Aaltonen *et al.* (CDF Collaboration), Phys. Rev. D **83**, 031102 (2011).
[41] T. Aaltonen *et al.* (CDF Collaboration), Phys. Rev. Lett. **103**, 041801 (2009).
[42] T. Aaltonen *et al.* (CDF Collaboration), Phys. Rev. D **77**, 051102 (2008).
[43] CMS Collaboration, Report No. CMS-PAS-EXO-11-092 (2012).
[44] G. Aad *et al.* (ATLAS Collaboration), arXiv:0901.0512.
[45] C. Adam Bourdarios *et al.* (ATLAS Collaboration), Report No. aTL-PHYS-PUB-2009-063.